Chemical Geology 427 (2016) 98–108

Contents lists available at ScienceDirect

Chemical Geology

journal homepage: www.elsevier.com/locate/chemgeo

Climate change and response in bottom water circulation and sediment provenance in the Central Arctic Ocean since the Last Glacial

A.-K. Meinhardt [a,*], K. Pahnke [b], P. Böning [b], B. Schnetger [a], H.-J. Brumsack [a]

[a] Microbiogeochemistry, Institute for Chemistry and Biology of the Marine Environment (ICBM), Carl von Ossietzky University Oldenburg, P.O. Box 2503, 26111 Oldenburg, Germany
[b] Max Planck Research Group for Marine Isotope Geochemistry, Institute for Chemistry and Biology of the Marine Environment (ICBM), Carl von Ossietzky University Oldenburg, P.O. Box 2503, 26111 Oldenburg, Germany

ARTICLE INFO

Article history:
Received 23 July 2015
Received in revised form 15 February 2016
Accepted 16 February 2016
Available online 18 February 2016

Keywords:
Arctic circulation
Provenance
Neodymium isotopes
Strontium isotopes

ABSTRACT

In this study, Arctic Ocean patterns of deep water circulation and sediment provenance during the Last Glacial (LG) were compared with the recent situation by investigating the Nd and Sr isotopic composition ($^{143}Nd/^{144}Nd$, expressed as ε_{Nd}, $^{87}Sr/^{86}Sr$) of the leachable and lithogenic sediment fractions as well as the elemental composition (Mn, Ca, Mg, total inorganic carbon (TIC)) on a spatially extended scale encompassing 11 sediment cores from several Arctic Ocean basins and ridges.

The leachable, authigenic signature of the surface sediments implies a North Atlantic deep water source and a late Holocene circulation regime that leads to well-mixed, mostly uniform, ε_{Nd} values of −10.9 to −10.3. Sediments from the LG have overall more variable authigenic ε_{Nd} values (−13.9 to −7.4). Lower values specifically occur in the Amerasian and Amundsen Basins, documenting an enhanced flow of deep waters from the Makarov Basin to the Amundsen Basin probably via the Lomonosov Ridge intra-basin.

In terms of detrital provenance areas, the lithogenic material deposited at the core locations cannot be unambiguously assigned to distinct source areas based on its radiogenic isotope composition, but represents a diverse mixture. Nevertheless, the Nd and Sr isotope signatures of surface sediments from the Amerasian Basin are dominated by western Arctic sources (ε_{Nd} = −12.8 to −11.0; $^{87}Sr/^{86}Sr$ = 0.7214 to 0.7251), while Eurasian Basin surface sediments are dominated by Eurasian sources (ε_{Nd} = −10.9 to −9.7, $^{87}Sr/^{86}Sr$ = 0.7178 to 0.7299), which is in agreement with previous studies. Bulk element patterns (Ca, Mg, TIC) of the studied sediments support these differences in provenance. The LG samples show the same trends with low ε_{Nd} (−16.1 to −13.7) and high $^{87}Sr/^{86}Sr$ (0.7294) in the Canada Basin, and higher ε_{Nd} (−12.6 to −8.8) and lower $^{87}Sr/^{86}Sr$ (0.7154 to 0.7249) in the Eurasian Basin sediments. However, LG samples have mostly lower and more heterogenous ε_{Nd} and $^{87}Sr/^{86}Sr$ values than the surface samples.

Our geochemical study shows that the overall circulation pattern of the deep water masses during the LG was locally influenced by brine formation but was generally similar to today. The isotopic composition of the lithogenic material from the LG is different from modern times, presumably due to shorter transport pathways of lithogenic material to the Arctic Ocean because of a lower sea level and exposed shelves during the LG. Nevertheless, the lithogenic fraction still represents a mixture from several sources.

1. Introduction

The deep water circulation of the Arctic Ocean is very important for the global climate because it impacts North Atlantic deep water formation and therefore forms a crucial part of the global overturning circulation (Aagaard et al., 1985). A varying Arctic deep water circulation during the Last Glacial (LG) may have contributed to the drop in global temperatures by decreasing the transport of heat around the global ocean (e.g., Broecker and Denton, 1989; Driscoll and Haug, 1998).

Information about water mass circulation in the oceans can be derived from Nd isotopes. Depending on lithology and age, continents have different isotopic signatures ($^{143}Nd/^{144}Nd$, expressed as ε_{Nd}) and these signatures are imprinted on sea water by weathering and erosion (e.g., Frank, 2002). The Nd isotopic composition of the authigenic Fe–Mn oxide fraction obtained by sequential leaching represents the Nd fraction, which is exchangeable with seawater, and thus reflects the dissolved deep water signal at the time of deposition (Rutberg et al., 2000; Bayon et al., 2002; Gutjahr et al., 2007). In the Arctic Ocean, several authors have investigated the Nd isotopic composition of authigenic sediment fractions (Winter et al., 1997; Haley et al., 2008a, 2008b; Maccali et al., 2013; Jang et al., 2013). It has been shown that the past deep

* Corresponding author.
E-mail address: ann.katrin.meinhardt@uni-oldenburg.de (A.-K. Meinhardt).

http://dx.doi.org/10.1016/j.chemgeo.2016.02.019

water circulation varied over glacial/interglacial timescales with some excursions due to specific events (e.g., outburst of ice-dammed lakes, melting of ice sheets; Spielhagen et al., 2004; Jakobsson et al., 2014). Haley and Polyak (2013) made the first attempt to use Nd isotopes on a broader spatial scale and defined a "pre-anthropogenic baseline" of deep water circulation in the Arctic Ocean. In our study we follow this approach and use the recent deep water circulation signals of surface sediments from several Arctic basins and ridges to update and refine this baseline. Additionally, we define the authigenic Nd isotopic composition of the last glacial to determine the glacial deep water circulation pattern on a broad spatial scale.

In order to better understand the environmental conditions in the Arctic and their impact on, and significance for, the Arctic Ocean during the LG compared to the modern, we studied the provenance of the lithogenic material using elemental concentrations and Nd and Sr isotopes. Investigation of sediment provenance in the Arctic is expected to reveal surface circulation patterns because sea ice drift forms the dominant distribution pathway of detritus from the Arctic coasts and shelves across the entire basin. It is therefore instrumental to use sediment archives to reconstruct sea ice patterns in different regions of the Arctic Ocean in order to compare LG and modern conditions.

The Arctic Ocean is surrounded by a large variety of lithologies, whose Nd and Sr isotopic compositions have mostly been determined. Therefore, distinct source areas can be defined. Our results provide a spatial and temporal pattern of sediment input and offer insight into the environmental conditions in the Arctic during the LG compared to the modern situation.

We hypothesize that glacial sediment provenance was different from today because of a lower sea level, exposed shelves, the existence of large ice sheets, and an overall more arid climate (e.g., Darby et al., 2006). Today the surface circulation in the Arctic Ocean is dominated by two major current systems: The anti-cyclonic Beaufort Gyre (BG) in the Amerasian Basin, and the Transpolar Drift (TPD) originating from the Siberian shelves and crossing the Arctic Ocean towards the Fram Strait. These currents transport sea ice – and sediments entrained in it – from the shelves across the entire Arctic Ocean. With our geochemical approach, we try to evaluate the potentially varying influence of these current systems on the isotopic signal of the studied sediments under last glacial and modern conditions. This will lead to a better understanding of present and past environmental conditions in the Arctic Ocean.

2. Material and methods

During R/V *Polarstern* expedition ARK-XXVI/3 in 2011 (Schauer, 2012), 11 multicorer cores were collected (Fig. 1a, Table 1; here referred to as 201, 206, 211, 217, 225, 231, 237, 248, 275, 277, and 285). Shortly after core recovery, sampling was carried out at a depth resolution of 1 cm and sediment slides were stored at ~4 °C. After freeze-drying on shore, the samples were finely ground in an agate ball mill for the determination of element concentrations. Isotopic measurements were done on the untreated bulk sediment.

2.1. Major and trace elements

Analyses of Al, Ca, Mg, and Mn concentrations were performed by wavelength-dispersive X-ray fluorescence (XRF, Philips PW 2400) on fused borate glass beads (detailed procedure in data repository of Eckert et al., 2013). Total inorganic carbon (TIC) was measured coulometrically with an UIC Coulometer. Accuracy and precision were checked with several inhouse standards (CAST, ICBM-B, Loess, PS-S, Peru, WAP; for TIC only Loess was used). For TIC, accuracy and precision were <1 rel-% (1σ). For XRF measurements, accuracy and precision were <4 rel-% (1σ). The water content of each sample, determined as the difference of wet and dry sediment weight, was used to correct the sediment content for each sea salt constituent to eliminate dilution effects resulting from sea salt enclosed in interstitial waters.

Element contents are displayed in weight % for major elements, ppm (μg/g) for trace elements, and are typically normalized to Al whose origin is essentially terrigenous and which is not affected by biogenic or

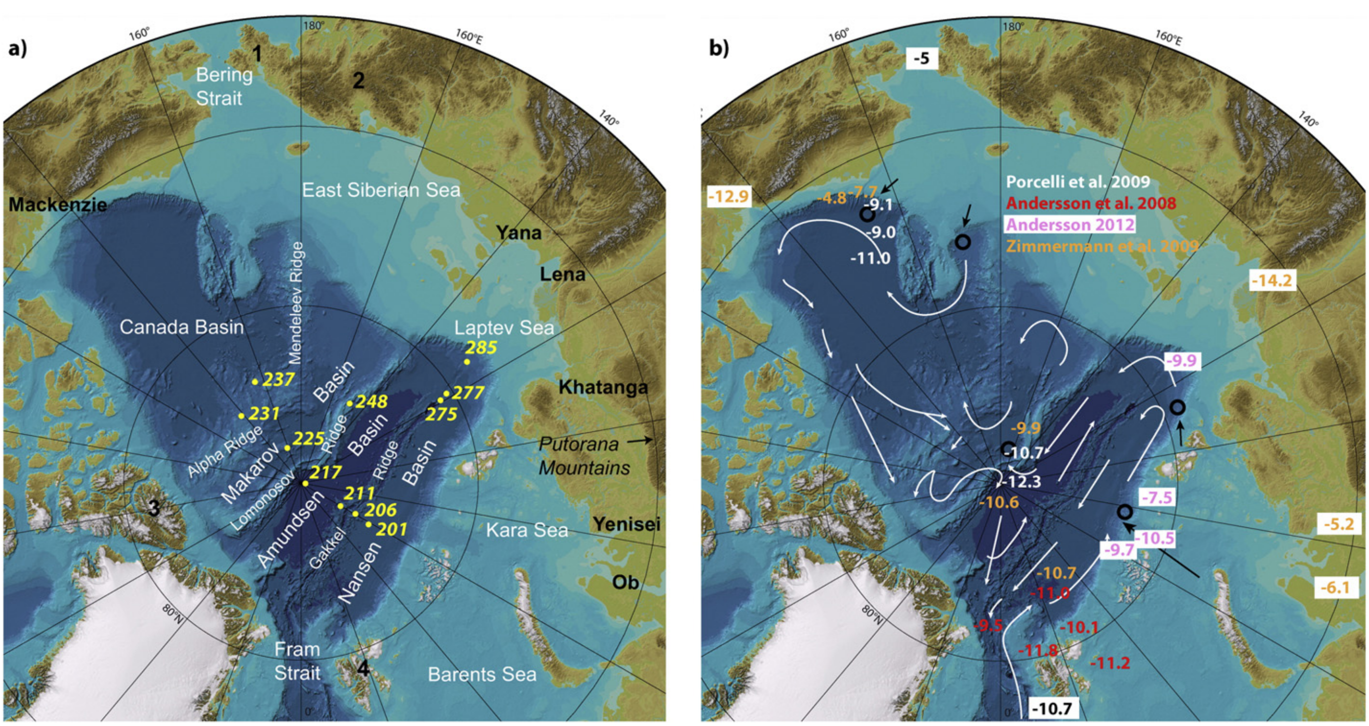

Fig. 1. (based on IBCAO, Jakobsson et al., 2008) a) Map of the Arctic Ocean with core locations and major rivers. Black numbers: 1: Chukchi Peninsula 2: Okhotsk–Chukotka volcanic belt 3: Arctic Archipelago; 4: Svalbard. b) Recent deep water currents (adapted from Rudels et al., 2012), literature values for deep water ε_{Nd} and river water ε_{Nd}. Black circles and arrows: possible sites of slope convection from cold, brine enriched shelf waters to the deep waters (Nansen, 1906; Rudels et al., 2012). Black numbers: Atlantic inflow from the Greenland Sea deep water (Piepgras and Wasserburg, 1987) and Pacific inflow (Dahlqvist et al., 2007).

diagenetic processes (Brumsack, 2006). Therefore, variable dilution of the terrigenous background can be excluded.

2.2. Nd and Sr isotopes

Sample preparation for Nd and Sr isotope analysis was modified from Chester and Hughes (1967). All chemicals were of ultrapure or distilled quality. Authigenic Fe–Mn oxides were leached from 500 mg of the bulk sediments using 10 ml of a 0.02 M solution of hydroxylamine hydrochloride (HH) in a weak 2% acetic acid matrix. The mixture was shaken for 1.5 h. After centrifuging, the supernatant was collected, centrifuged again, filled into a Teflon beaker and dried down at 160 °C. The samples were dissolved in 0.5 ml 1 N HNO_3 for separation of rare earth elements (REE) from Sr and other cations on Eichrom Tru-Spec resin (100–150 μm mesh; Pin and Zalduegui, 1997). Final isolation of Nd from other REE was achieved using Eichrom Ln-Spec resin (50–100 μm mesh; Pin and Zalduegui, 1997) and 0.24 N HCl as eluant. The residual sediment fraction (after the first leach, see above) was washed with demineralized water and then treated with 10 ml of buffered acetic acid (pH of 5.5) to remove carbonates. The suspension was agitated over night. After centrifuging, the supernatant was discarded and the sediment was again washed with demineralized water. The carbonate removal was repeated until no more CO_2 was released, followed by two more leaching steps with HH (0.02 M in 25% acetic acid, 6 h and 24 h) to remove any authigenic fraction.

Complete digestion was performed with about 40 mg of the residual detrital sediment fraction, 0.5 ml conc. $HClO_4$, 3 ml conc. HF, and 3 × 3 ml 6 M HCl. Pure MgO powder was added in excess (~20 mg) prior to dissolution to prevent the formation of AlF_3 (Takei et al., 2001). For separation of REEs from Sr and other cations, Eichrom Tru-Spec resin was used. The isolation of Nd followed the procedure described above, while Sr was isolated from Rb using Eichrom Sr-Spec resin (100–150 mm mesh).

Neodymium and Sr isotopes were measured with a multi-collector ICP-MS (Neptune Plus, Thermo Scientific) at the University of Oldenburg. For Nd isotope analyses, all samples were corrected for mass fractionation using $^{146}Nd/^{144}Nd = 0.7219$ and an exponential law. Each measurement session was accompanied by multiple analyses of the Nd standard JNdi-1 (generally every 3 samples), and $^{143}Nd/^{144}Nd$ ratios of all samples were normalized to the reported JNdi-1 value of $^{143}Nd/^{144}Nd = 0.512115$ (Tanaka et al., 2000). The Nd isotopic composition is expressed in ε_{Nd} notation:

$$\varepsilon_{Nd} = [(^{143}Nd/^{144}Nd)_{sample}/(^{143}Nd/^{144}Nd)_{CHUR} - 1] * 10^4.$$

where $(^{143}Nd/^{144}Nd)_{CHUR}$ is the Chondritic Uniform Reservoir with a value of 0.512638 (Jacobsen and Wasserburg, 1980).

Typical long-term external errors (reported as 2σ SD, Table 1) range between 0.16 and 0.33 ε_{Nd}, based on multiple JNdi-1 analyses during each session (n = 6–8). The BCR-2 standard had an ε_{Nd} value of 0.1 (±0.3; n = 5; 2σ), which is well within the reported ε_{Nd} value of 0.0 ± 0.2 (Raczek et al., 2003). The addition of MgO to the acid digestion resulted in Nd blank levels of 2–4% of sample Nd. To check the potential influence of the MgO powder on the isotopic ratios of the samples, five MgO powder samples were treated the same way as the samples. These MgO blanks yielded ε_{Nd} values of −11.1 ± 0.5 to −8.5 ± 0.5. Using a simple mixing calculation, the maximum influence of the MgO powder on the isotopic composition of the samples was +0.1 ε_{Nd} units. This is in the range of the analytical uncertainty of the sample measurements and can therefore be neglected.

For Sr isotope analyses, all samples were corrected for mass fractionation using $^{86}Sr/^{88}Sr = 0.1194$ and the exponential law. Measurements were accompanied by multiple analyses of NBS987 (generally every 7 samples), and $^{87}Sr/^{86}Sr$ values of all samples were normalized to the reported NBS987 value of 0.710248 (Thirlwall, 1991). Krypton 'gas blanks' measured on ^{83}Kr and used to correct for ^{86}Kr on ^{86}Sr were below 0.1 mV (while ^{86}Sr was measured at 2–3 V) and are therefore negligible. Rubidium and Ba contents were also found to be negligible. Typical long-term external errors (reported as 2σ SD, Table 1) range between 0.000021 and 0.000026 $^{87}Sr/^{86}Sr$, based on multiple NBS987 analyses during each session (n = 3–4). The BCR-2 standard had a $^{87}Sr/^{86}Sr$ value of 0.70504 ± 0.00002 (n = 5; 2σ), well within the reported value of 0.70496 (Raczek et al., 2003).

2.3. Sampling strategy for recent Holocene and LG sediment samples

The age of the sediments was estimated based on the Mn/Al variations of the sediment cores (Fig. 2). Close to the surface, the sediment cores show elevated Mn/Al ratios that decrease downcore until a minimum is reached. We chose the upper first centimeters of each core as a representative sample for recent Holocene sedimentation. As demonstrated by Meinhardt et al. (2014) for sediment cores from the Mendeleev Ridge, the first downcore minimum in Mn/Al reflects reduced fluvial and coastal erosion-derived Mn input during glacial periods (Jakobsson et al., 2000), and corresponds to the LG. Therefore we have chosen samples from the first Mn/Al minimum to represent the LG. We apply this stratigraphy under the assumption that the continental input factors controlling the Mn/Al on the Mendeleev Ridge are valid for other parts of the Arctic Ocean as well.

Conventional dating in Arctic Ocean sediments (e.g., ^{14}C dating, $\delta^{18}O$ stratigraphy) is limited because of poor preservation of calcareous nanofossils and the varying riverine fresh water input, which prevents the correlation of foraminiferal oxygen isotopes to lower latitude oxygen isotope records (Backman et al., 2004; Spielhagen et al., 2004). Stratigraphic correlation based on elevated Mn contents can be applied for central Arctic Ocean sediments when diagenetic remobilization can be excluded (März et al., 2011; Löwemark et al., 2014). In the studied multicorer samples, additional pore water analyses (not shown) reveal Mn^{2+} concentrations below detection limit, suggesting that diagenetic Mn relocation is negligible. The correlation may not be valid for all parts of the Arctic Ocean and we therefore refer to Mn-poor/cold/LG-like depositional conditions throughout the manuscript. Core 285 shows no variation in Mn/Al. Therefore we were not able to identify the LG in this core. In general the minima and maxima in cores from near the Laptev shelf are less pronounced. To constrain the applied stratigraphy additional age control should be provided in further studies.

3. Results

3.1. Geochemical characteristics of the sediment cores

Compared to average shale ("AS", Wedepohl, 1971, 1991), all cores are enriched in Mn at the surface with highest enrichments in core 217 from the North Pole (Amundsen Basin) and cores 231 and 237 from the Alpha Ridge/Canada Basin (Fig. 2, Table 2). The Mn/Al ratios decrease downcore towards lower ratios that mark the LG (Meinhardt et al., 2014), before they sharply increase towards a maximum. In cores close to the Laptev Sea shelf (275 to 285), the minima and maxima are less pronounced compared to the other locations.

The surfaces of cores 201, 206, 211, 231, and 237 are also enriched in Ca, and parallel enrichments in Ca, Mg, and TIC are visible in the upper centimeters of cores 231 and 237 (Fig. 3, Table 2).

3.2. Nd isotope ratios of authigenic Fe–Mn oxides (leachable fraction)

The Nd isotope signature of the surface sediment leachates is rather uniform. Except for station 201 in the Nansen Basin ($\varepsilon_{Nd} = -9.2$), the ε_{Nd} values range from −10.9 to −10.3 (Fig. 4a, Table 1).

The samples from the LG show larger spatial differences than the surface samples, with higher ε_{Nd} in the Nansen Basin (−8.8 to −7.4) and lower ε_{Nd} in the Canada (−13.9) and Amundsen Basins (−12.2

Table 1
Core locations, bulk element contents and Nd and Sr isotopic composition of the leachable and lithogenic fractions of modern and LG (bold) samples.

					Leachable fraction					Lithogenic fraction	
Station	Latitude	Longitude	Water depth (m)	Depth in core (cm)	$^{143}Nd/^{144}Nd$ [a]	Internal error (2σ SE)	ε_{Nd}	external Error (ε_{Nd}, 2σ SD)	Propagated error (ε_{Nd}) [b]	$^{143}Nd/^{144}Nd$ [a]	Internal error (2σ SE)
PS78/201-7	85° 32.49′ N	59° 25.01′ E	3797	0–1	0.512167	0.000012	−9.2	0.16	0.29	0.512138	0.000003
				2–3	**0.512185**	**0.000005**	**−8.8**	**0.33**	**0.35**	**0.512119**	**0.000005**
PS78/206-2	86° 26.43′ N	60° 5.75′ E	1770	0–1	0.512100	0.000013	−10.5	0.16	0.29	0.512106	0.000006
				6–7	**0.512258**	**0.000003**	**−7.4**	**0.33**	**0.34**	**0.512185**	**0.000009**
PS78/211-1	87° 36.04′ N	61° 3.23′ E	4026	0–1	0.512082	0.000004	−10.9	0.16	0.17	0.512080	0.000014
				7–8	**0.512054**	**0.000012**	**−11.4**	**0.33**	**0.41**	**0.512060**	**0.000012**
PS78/217-1	89° 57.73″ N	97° 41.59′ E	4122	0–1	0.512111	0.000003	−10.3	0.16	0.17	0.512128	0.000009
				21–22	**0.512017**	**0.000007**	**−12.1**	**0.33**	**0.36**	**0.511993**	**0.000010**
PS78/225-4	87° 39.09′ N	157° 43.61′ W	2314	0–1	0.512096	0.000012	−10.6	0.16	0.27	0.512077	0.000011
				4–5	**0.512049**	**0.000012**	**−11.5**	**0.33**	**0.41**	**0.512062**	**0.000020**
PS78/231-1	84° 54.32′ N	137° 48.54′ W	1594	0–1	0.512096	0.000011	−10.6	0.16	0.26	0.512026	0.000005
				2–3	**0.512014**	**0.000003**	**−12.2**	**0.33**	**0.34**	**0.511938**	**0.000006**
PS78/237-1	83° 44.65′ N	154° 24.88′ W	2378	0–1						0.511982	0.000008
				5–6	**0.511923**	**0.000009**	**−13.9**	**0.33**	**0.38**	**0.511814**	**0.000012**
PS78/248-4	84° 40.75′ N	149° 59.41′ E	1611	0–1	0.512112	0.000007	−10.3	0.16	0.21	0.512127	0.000012
				19–20	**0.512099**	**0.000006**	**−10.5**	**0.18**	**0.21**	**0.512088**	**0.000015**
PS78/275-1	80° 49.13′ N	120° 58.26′ E	3527	0–1	0.512101	0.000009	−10.5	0.16	0.23	0.512096	0.000007
				18–19	**0.512101**	**0.000006**	**−10.5**	**0.18**	**0.21**	**0.512070**	**0.000005**
PS78/277-2	80° 12.54′ N	122° 12.20′ E	3359								
				19–20	**0.512104**	**0.000004**	**−10.4**	**0.33**	**0.34**	**0.512067**	**0.000014**
PS78/285-6	78° 29.97′ N	125° 42.94′ E	2805	0–1	0.512112	0.000010	−10.3	0.16	0.26	0.512116	0.000004

[a] Normalized to the JNdi $^{143}Nd/^{144}Nd$ value of 0.512115 (Tanaka et al., 2000).
[b] $\sqrt{(\text{internal error})^2 + (\text{external error})^2}$.
[c] Normalized to the NBS987 $^{87}Sr/^{86}Sr$ value of 0.710248 (Thirlwall, 1991).

to −11.4) (Fig. 4b). Samples from the Lomonosov Ridge and near the Laptev shelf have values similar to the surface samples.

3.3. Nd and Sr isotopes of the terrigenous fraction

To distinguish between different source areas of the terrigenous material, we plot our Nd and Sr isotope results into ε_{Nd} versus $^{87}Sr/^{86}Sr$ diagrams together with Nd and Sr isotope compositions of the surrounding Arctic terrains as potential source endmembers (Fig. 5). The lithogenic fraction of the surface samples shows ε_{Nd} values of −12.8 to −9.7 (Figs. 5a, 6a; Table 1). The most negative values are found in samples closer to the Canadian Arctic (cores 231 and 237). The $^{87}Sr/^{86}Sr$ values from the terrigenous fraction of the surface sediments range from 0.7154 to 0.7299 (Fig. 5a, Table 1). Fig. 4a shows, that no sample can be assigned to one distinct source area but that they plot between potential source areas. The $^{87}Sr/^{86}Sr$ values of cores from the Eurasian Basin (206, 211, 275, 285) are located closer to the suspended particulate matter (SPM) of the Siberian rivers Khatanga, Yana, and Lena than samples 231 and 237 from the Amerasian Basin. Some distinct trends are visible for the surface sediments. Cores 231 and 237 from the Alpha Ridge/ Canada Basin have the lowest ε_{Nd} values of the surface sediments and plot closer to the Mackenzie particles. This is in accordance with their geographic location: Of all cores they are located closest to the North American continent. Core 201 from the Nansen Basin, which is located nearest to Svalbard, has the highest ε_{Nd} and $^{87}Sr/^{86}Sr$ values. Core 206 from the southern Gakkel Ridge has the lowest $^{87}Sr/^{86}Sr$ value. Cores 211 from the northern Gakkel Ridge, 225 from the Makarov Basin, and 275 and 285 near the Laptev shelf plot closely together.

During the LG, ε_{Nd} values are mostly in the same range as the surface samples, except for core 206 with higher ε_{Nd} (−8.8) and cores 231 and 237 with lower ε_{Nd} (−13.7 and −16.1, respectively; Table 1). The most negative values are again found in the Canada Basin. Most of the LG samples have lower ε_{Nd} values and lower $^{87}Sr/^{86}Sr$ values than the surface samples, but these differences are quite small (Fig. 7).

4. Discussion

4.1. Bulk sediment characteristics

In the oxic environment of the Arctic Ocean, Mn forms (oxyhydr)oxides with a high adsorption capacity for many elements. High enrichments of Mn are common in Arctic Ocean sediment cores (e.g., Jakobsson et al., 2000; März et al., 2011; Macdonald and Gobeil, 2012; Löwemark et al., 2014; Meinhardt et al., 2014). In the Central Arctic Ocean, dark brown, Mn-rich sediment layers alternate with lighter olive brown, Mn poor layers. The main reason for the occurrence of these Mn layers is the enhanced input from rivers and coastal erosion during interglacial/interstadial times (Jakobsson et al., 2000; Macdonald and Gobeil, 2012).

The very high Mn/Al values especially in the surface samples of cores 231 and 237 may result from either enhanced fluvial/erosional Mn input in the recent warm period compared to the LG or enhanced diagenetic remobilization. Riverine input has been found to dominate over coastal erosion in the Canadian Beaufort Sea, and coastal erosion may only be important locally (Rachold et al., 2000). Secondary processes may redistribute Mn in the sediment after deposition (Li et al., 1969; Macdonald and Gobeil, 2012), but this can be excluded for surface sediments in the central Arctic Ocean (Meinhardt et al., in review).

The enrichment in Ca in the upper intervals of sediment cores 231 and 237 indicates the presence of biogenic or terrigenous detrital carbonate (Fig. 3). Terrigenous carbonates (mostly dolomite) are characterized by synchronous enrichments in Ca, Mg, and TIC, as seen in the surface samples of the two sediment cores and the LG sample of core 237. Dolomite is common in the western part of the Arctic and presumably originates from the Arctic Archipelago (Banks and Victoria Islands, Bischof et al., 1996; Bischof and Darby, 1997). It is transported by icebergs and sea ice as ice rafted debris (IRD) with the BG in the western Arctic Ocean. The element profiles therefore give evidence that locations 231 and 237 have been influenced by the BG and that TIC is indicative for Arctic Archipelago provenance. However, dolomite is not indicative for changes between modern and LG conditions and can only be used for sediments from the Amerasian Basin.

Station	Lithogenic fraction							Bulk sediment				
	ε_{Nd}	External error (ε_{Nd}, 2σ SD)	Propagated error (ε_{Nd})[b]	$^{87}Sr/^{86}Sr$[c]	Internal error (2σ SE)	External error (2σ SE)	Propagated error[b]	Mn (%)	Al (%)	Mg (%)	Ca (%)	Mn/Al
PS78/201-7	-9.7	0.25	0.26	0.72991	0.000017	0.000024	0.000029	0.256	9.60	1.86	1.40	0.027
	-10.1	**0.25**	**0.27**	**0.72492**	**0.000028**	**0.000026**	**0.000038**	**0.164**	**9.66**	**1.80**	**1.31**	**0.017**
PS78/206-2	-10.4	0.25	0.28	0.71785	0.000017	0.000024	0.000029	0.217	7.02	1.06	3.31	0.031
	-8.8	**0.25**	**0.31**	**0.71542**	**0.000019**	**0.000026**	**0.000033**	**0.081**	**7.39**	**1.03**	**1.13**	**0.011**
PS78/211-1	-10.9	0.25	0.37	0.72038	0.000002	0.000024	0.000024	0.510	8.29	1.44	2.64	0.062
	-11.3	**0.18**	**0.29**	**0.71720**	**0.000003**	**0.000026**	**0.000027**	**0.331**	**8.64**	**1.42**	**1.51**	**0.038**
PS78/217-1	-9.9	0.25	0.30	0.72243	0.000009	0.000024	0.000026	0.658	8.53	1.72	1.37	0.077
	-12.6	**0.18**	**0.26**	**0.72190**	**0.000012**	**0.000026**	**0.000029**	**0.137**	**9.55**	**1.70**	**0.65**	**0.014**
PS78/225-4	-11.0	0.25	0.33	0.72135	0.000020	0.000024	0.000031	0.580	8.83	1.58	1.53	0.066
	-11.2	**0.25**	**0.47**	**0.72140**	**0.000003**	**0.000021**	**0.000021**	**0.355**	**7.51**	**2.09**	**4.53**	**0.047**
PS78/231-1	-11.9	0.25	0.27	0.72512	0.000003	0.000024	0.000024	0.403	5.06	2.39	10.81	0.080
	-13.7	**0.25**	**0.28**	**0.72240**	**0.000012**	**0.000021**	**0.000024**	**0.286**	**4.80**	**2.94**	**12.28**	**0.060**
PS78/237-1	-12.8	0.25	0.28	0.72466	0.000011	0.000024	0.000026	0.385	5.50	2.36	9.82	0.070
	-16.1	**0.25**	**0.35**	**0.72943**	**0.000018**	**0.000026**	**0.000032**	**0.182**	**4.44**	**4.23**	**12.12**	**0.041**
PS78/248-4	-10.0	0.25	0.35	0.71937	0.000026	0.000024	0.000036	0.565	8.60	1.57	1.65	0.066
	-10.7	**0.25**	**0.39**	**0.71657**	**0.000013**	**0.000026**	**0.000029**	**0.339**	**9.00**	**1.37**	**0.81**	**0.038**
PS78/275-1	-10.6	0.25	0.29	0.72037	0.000008	0.000024	0.000025	0.396	8.12	1.45	2.28	0.049
	-11.1	**0.25**	**0.27**	**0.71609**	**0.000010**	**0.000026**	**0.000028**	**0.189**	**8.79**	**1.34**	**0.68**	**0.022**
PS78/277-2								0.413	8.51	1.49	1.99	0.049
	-11.1	**0.25**	**0.37**	**0.71667**	**0.000025**	**0.000026**	**0.000036**	**0.212**	**8.78**	**1.39**	**0.71**	**0.024**
PS78/285-6	-10.2	0.18	0.19	0.72049	0.000005	0.000024	0.000024	0.384	8.70	1.64	1.36	0.044

Samples from the LG have higher Mn contents than the local background, indicating the occurrence of additional authigenic Mn to the sediment even during the glacial period. But they generally have lower Mn contents than the modern samples due to reduced fluvial and erosional input. However, the authigenic sediment fraction is very large and biases the use of other bulk sedimentary trace metals as provenance indicators (e.g., Ni, Y), leading to ambiguous results. To avoid this bias we will focus on the Nd and Sr isotopic composition of the lithogenic sediment fraction after removal of the authigenic sediment fraction for provenance studies (Chapter 4.3).

4.2. Nd isotope ratios of authigenic Fe–Mn oxides

4.2.1. Modern situation

Atlantic inflow is the primary source of Arctic Ocean deep water (Fig. 1b) with an ε_{Nd} signature of −10.7 (from the Greenland Sea deep water, Piepgras and Wasserburg, 1987). The surface samples from the Eurasian Basin (except for core 201 with ε_{Nd} − 9.2, discussed below) show values of ε_{Nd} − 10.6 ± 0.3, supporting the dominating influence of bottom water from the North Atlantic. This is in accordance with previous studies (e.g., Haley and Polyak, 2013) and suggests well-mixed deep waters with an Atlantic origin in the Eurasian part of the Arctic Ocean.

Core 201 in the Nansen Basin is the only one with a slightly higher ε_{Nd} value of −9.2, the same as a sediment sample from the Kara shelf (Haley and Polyak, 2013; Fig. 4a). This may indicate the influence of shelf-seawater interaction and the transport of this signal into deep waters through brine formation or minor redeposition of particles with coatings formed on the Kara Sea shelf.

The Nd isotope ratios of cores 275 and 285 near the Laptev Sea shelf (ε_{Nd} − 10.5 and −10.3, respectively) show the North Atlantic ε_{Nd} signature and clearly differ from sediments directly on the shelf (ε_{Nd} = −8.8 to −8.0, Haley and Polyak, 2013, Fig. 4a). This indicates that there is no direct transport of waters from the shelf to the deep basin in this region (as would be expected in case of brine rejection).

One deep water measurement of Porcelli et al. (2009) in the Amundsen Basin shows an ε_{Nd} value of −12.3 (Fig. 1b), which is considerably lower than elsewhere in the Arctic Ocean. The authors explain this value by exchange between shelf sediments and overlying waters. They doubt simple mixing of North Atlantic derived water with shelf water or addition of Nd as explanation for lower values in the Amundsen Basin. Our data do not confirm this finding. Core 217 from the Amundsen Basin has a similar ε_{Nd} (−10.3) as our other surface samples in the Eurasian Basin and the value of Zimmermann et al. (2009) from the Amundsen Basin (Fig. 1b), suggesting that this location is as well influenced by well-mixed deep water with a North Atlantic origin.

Pacific water enters the Arctic Ocean with an average ε_{Nd} value of ~ −5 (Dahlqvist et al., 2007). Even core 237 closest to the Canada Basin shows no change towards more positive values and is therefore apparently not influenced by Pacific water.

4.2.2. Last Glacial

The ε_{Nd} results from the LG show a less homogenous deep water ε_{Nd} distribution in the Arctic Ocean compared to the modern situation, most likely suggesting stronger local influence due to more sluggish deep water circulation (Fig. 4b). During the LG, the sea level was lower than today and most of the Siberian shelf area was exposed. The core sites were therefore subject to more direct influence by rivers and brine rejection. Water from the Pacific Ocean with a more positive isotopic signature could not enter the Arctic Ocean.

Location 237 with a low ε_{Nd} signature (−13.9) must have been influenced by water with a more negative signature. One possible source with negative signature is the Mackenzie River (ε_{Nd} = −12.9), whose isotopic signature is transported with the anti-cyclonic BG in the Canada Basin. Its isotopic signature must have been even more negative during the LG by at least one ε_{Nd} unit to cause the observed signal. In sediments close to the North Pole, Haley et al. (2008a) explained low ε_{Nd} values during glacial intervals with brine formation occurring on the Eurasian shelves. The isotopic signature of the Lena River (ε_{Nd} = −14.2) is a potential source for low ε_{Nd} values and may be added to the deep water through brine rejection.

A higher ε_{Nd} signal is seen in Nansen Basin samples from cores 201 and 206 (ε_{Nd} values of −8.8 and −7.4, respectively), possibly indicating local river input to surface waters or partial dissolution of riverine particles and subsequent brine rejection. A possible source for higher ε_{Nd} values on land are the Putorana Mountains. Material from the Putorana

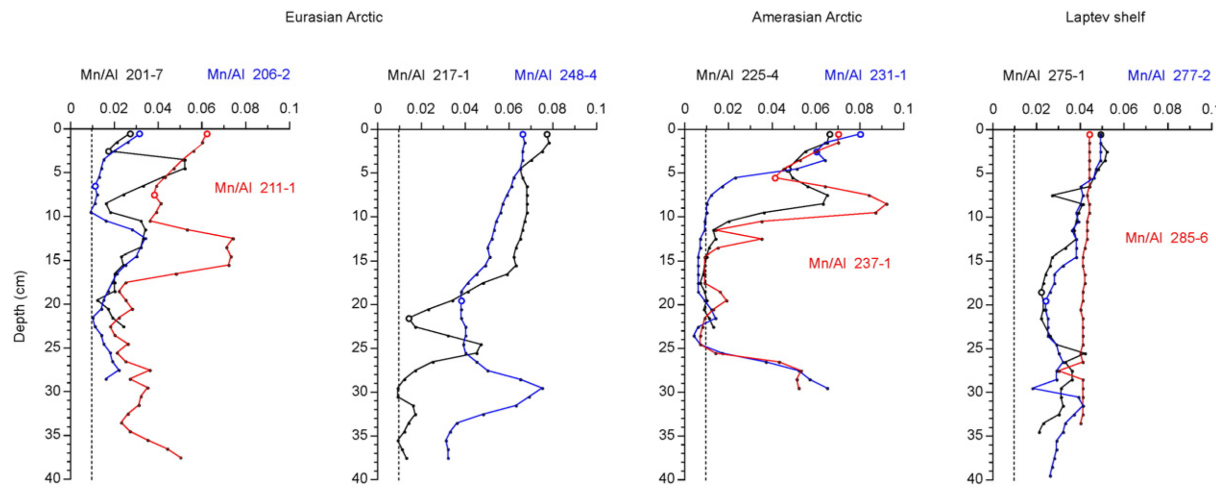

Fig. 2. Mn/Al ratios of the studied multicorer cores. Open circles mark samples for isotope measurements. Dashed line marks average shale (Wedepohl, 1971, 1991).

Mountains ($\varepsilon_{Nd} \geq 0$, Sharma et al., 1992), which is transported by rivers and coastal erosion to the shelf area, is incorporated into the Eurasian ice sheet. This ice sheet extended to the current shelf edge of the Kara and Barents Seas (Svendsen et al., 2004). Boundary exchange and brine rejection on the ice edge especially in the Kara Sea may have transferred this material to the deeper waters, as proposed by Aagaard et al. (1985); Tütken et al. (2002), and Haley et al. (2008a). As the deep water from the Nansen Basin with its higher ε_{Nd} flows towards the Laptev shelf, it must have mixed with local water with a lower ε_{Nd} signature along its way, because samples from the Lomonosov Ridge (core 248) and near the Laptev shelf (core 275 and 277) have lower ε_{Nd} values (−10.5 to −10.4) than cores 201 and 206 (−8.8 to −7.4).

Table 2
Mn/Al of all studies cores; Mg/Al, Ca/Al, and TIC (%) of cores 231-1 and 237-1.

	201-7	206-2	211-1	217-1	225-4	231-1				237-1				248–4	275–1	277–2	285–6
Depth (cm)	Mn/Al	Mn/Al	Mn/Al	Mn/Al	Mn/Al	Mn/Al	Mg/Al	Ca/Al	TIC (%)	Mn/Al	Mg/Al	Ca/Al	TIC (%)	Mn/Al	Mn/Al	Mn/Al	Mn/Al
0–1	0.027	0.031	0.062	0.077	0.066	0.080	0.472	2.135	3.70	0.070	0.429	1.784	2.54	0.066	0.049	0.049	0.044
1–2	0.021	0.026	0.060	0.078	0.065	0.064	0.455	1.628	3.46	0.070	0.321	1.317	2.54	0.067	0.049	0.049	0.044
2–3	0.017	0.020	0.056	0.075	0.055	0.060	0.611	2.613	4.22	0.056	0.342	1.048	2.84	0.066	0.052	0.049	0.044
3–4	0.052	0.015	0.051	0.070	0.051	0.064	0.571	3.312	5.08	0.053	0.431	1.079	2.84	0.066	0.051	0.049	0.044
4–5	0.052	0.014	0.047	0.065	0.047	0.051	0.302	2.150	3.79	0.045	0.699	1.698	2.89	0.065	0.048	0.047	0.044
5–6	0.042	0.013	0.043	0.066	0.049	0.023	0.238	1.881	3.68	0.041	0.951	2.729	2.89	0.062	0.046	0.046	0.044
6–7	0.033	0.011	0.039	0.068	0.056	0.017	0.229	1.815	3.31	0.064	0.780	3.010	2.92	0.061	0.044	0.040	0.044
7–8	0.024	0.012	0.038	0.068	0.065	0.012	0.169	0.893	1.54	0.084	0.398	1.742	2.92	0.059	0.027	0.041	0.043
8–9	0.016	0.011	0.041	0.068	0.063	0.010	0.148	0.558	1.12	0.092	0.259	1.273		0.057	0.041	0.040	0.044
9–10	0.018	0.009	0.039	0.068	0.036	0.010	0.145	0.422	0.85	0.087	0.191	0.795	5.26	0.056	0.039	0.038	0.044
10–11	0.032	0.016	0.036	0.067	0.020	0.009	0.144	0.423	0.87	0.035	0.162	0.489		0.054	0.038	0.039	0.043
11–12	0.034	0.028	0.053	0.066	0.013	0.009	0.125	0.229		0.014	0.140	0.248		0.053	0.037	0.036	0.043
12–13	0.033	0.034	0.074	0.065	0.014	0.007	0.116	0.111	0.13	0.035	0.164	0.491		0.052	0.038	0.038	0.043
13–14	0.032	0.032	0.071	0.063	0.011	0.007	0.106	0.074		0.015	0.145	0.272	1.71	0.050	0.033	0.038	0.042
14–15	0.023	0.030	0.073	0.062	0.010	0.006	0.110	0.067	0.04	0.009	0.116	0.117		0.051	0.027	0.038	0.041
15–16	0.024	0.025	0.072	0.063	0.009	0.006	0.107	0.057		0.009	0.135	0.173		0.049	0.026	0.032	0.041
16–17	0.020	0.021	0.048	0.059	0.008	0.006	0.105	0.054	0.01	0.009	0.175	0.300		0.045	0.024	0.028	0.042
17–18	0.020	0.019	0.025	0.048	0.007	0.006	0.104	0.057		0.009	0.138	0.180		0.041	0.023	0.028	0.042
18–19	0.020	0.017	0.022	0.041	0.009	0.006	0.105	0.055	0.01	0.016	0.147	0.233		0.038	0.022	0.026	0.041
19–20	0.012	0.015	0.025	0.034	0.010	0.009	0.105	0.059		0.019	0.163	0.193		0.038	0.023	0.024	0.041
20–21	0.017	0.014	0.028	0.023	0.009	0.012	0.106	0.053	0.01	0.013	0.144	0.153		0.038	0.023	0.024	0.040
21–22	0.019	0.010	0.022	0.014	0.011	0.014	0.104	0.054		0.009	0.123	0.109		0.038	0.022	0.025	0.041
22–23	0.024	0.011	0.018	0.017	0.013	0.006	0.104	0.059	0.02	0.008	0.119	0.101		0.040		0.025	0.041
23–24		0.014	0.020	0.032		0.004	0.099	0.067		0.007	0.116	0.093		0.040	0.026	0.025	0.041
24–25		0.015	0.026	0.047		0.007	0.120	0.119	0.19	0.007	0.119	0.110		0.039	0.029	0.029	0.041
25–26		0.018	0.021	0.045		0.017	0.200	0.300		0.014	0.145	0.194		0.040	0.042	0.030	0.040
26–27		0.019	0.025	0.025		0.037	0.258	0.595	1.57	0.043	0.447	0.902		0.045	0.033	0.032	0.041
27–28		0.022	0.036	0.017		0.052	0.355	1.112		0.053	0.348	0.800		0.050	0.036	0.029	0.030
28–29		0.016	0.027	0.012		0.057	0.364	1.326	2.94	0.051	0.358	0.791		0.065	0.036	0.029	0.041
29–30			0.035	0.009		0.065	0.398	1.465		0.052	0.386	0.826		0.075	0.031	0.018	0.041
30–31			0.032	0.009										0.069	0.031	0.039	0.041
31–32			0.031	0.016										0.063	0.032	0.041	0.041
32–33			0.026	0.017										0.048	0.030	0.037	0.041
33–34			0.023	0.014										0.036	0.023	0.033	0.040
34–35			0.027	0.012										0.033	0.021	0.032	
35–36			0.035	0.009										0.031		0.029	
36–37			0.044	0.011										0.032		0.029	
37–38			0.050	0.013										0.032		0.028	
38–39																0.027	
39–40																0.026	

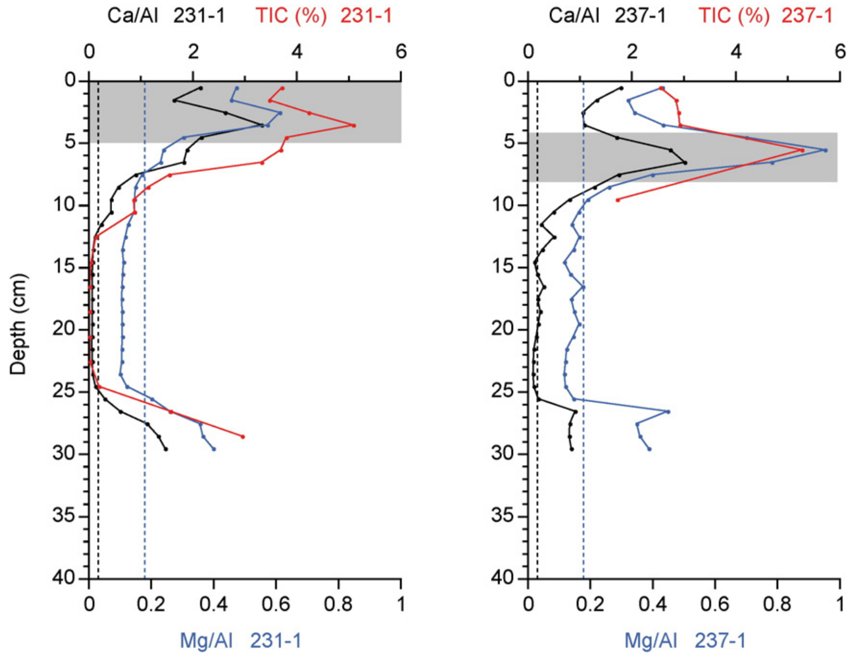

Fig. 3. Sedimentary Ca/Al (black), Mg/Al (blue), and TIC (red) data for cores 231 and 237 from the Canada Basin. Dashed lines: average shale. Gray bars indicate sediment layers with supposed occurrence of dolomite.

In this area, the Lena River is a likely source and could have had a greater influence than today. It has been found that the very low Lena water signature of −14 does not propagate far onto the Laptev shelf today, but is diluted on the shelf by coastal currents flowing eastward (Haley and Polyak, 2013). This dilution must have been absent during the LG because of the exposed shelf area, which moved the river mouth closer to the core location.

At the Northern Gakkel Ridge and the North Pole (stations 211 and 217), LG ε_{Nd} values (−12.2 and −11.4, respectively) are lower than the surface samples. This may indicate an enhanced water flow from the Makarov Basin through an intra-basin on the Lomonosov Ridge. This water flow has been observed in the modern Arctic Ocean (Björk et al., 2007) and may have been active during the LG as well. This is likely, because deep waters from the Canada and Makarov Basins (cores 225, 231, and 237) have low ε_{Nd} value of −13.9 to −11.5. A reverse flow from the Amundsen Basin to the Makarov Basin has not been observed by Björk et al. (2007).

Our results agree with Darby et al. (2006) who found enhanced water-mass exchange in the modern Arctic Ocean compared to the Last Glacial and with Bischof and Darby (1997) who found that North

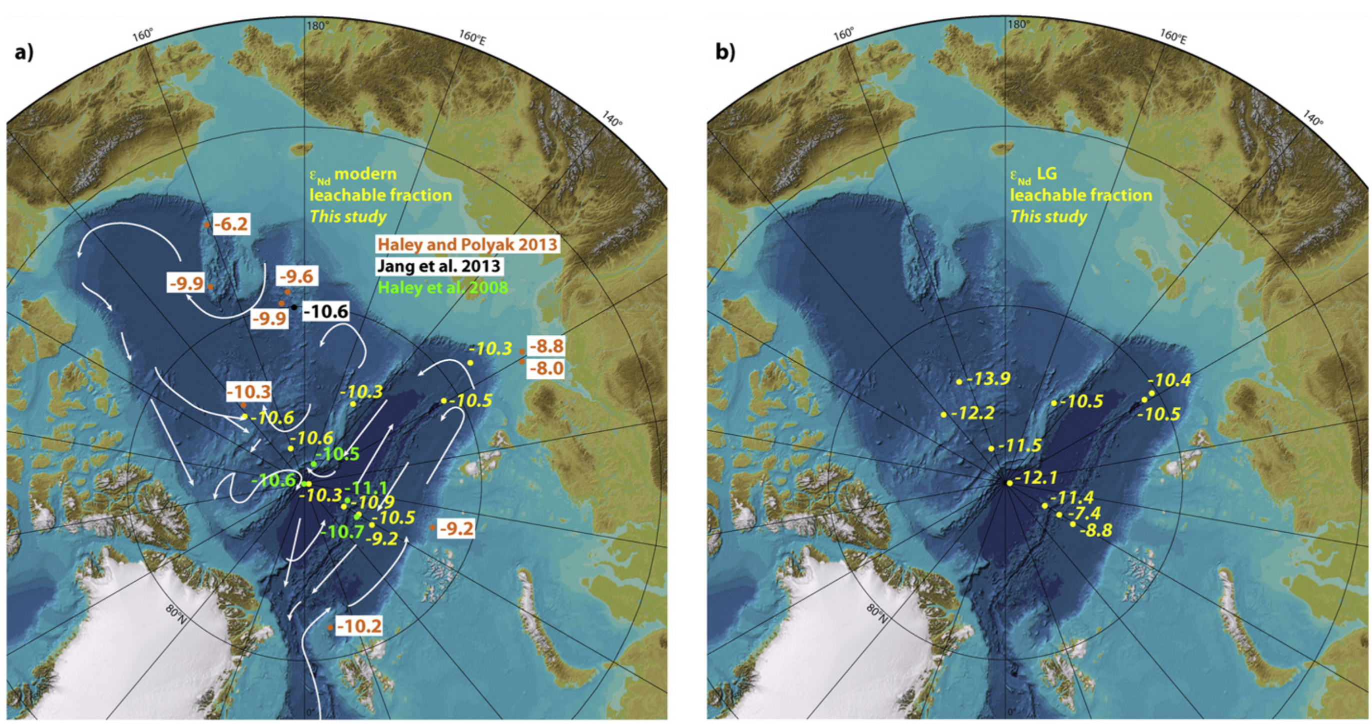

Fig. 4. (based on IBCAO, Jakobsson et al., 2008) ε_{Nd} values of the leachates from a) surface sediments, b) sediments from the Last Glacial. Additional literature values of sediment leachates are given.

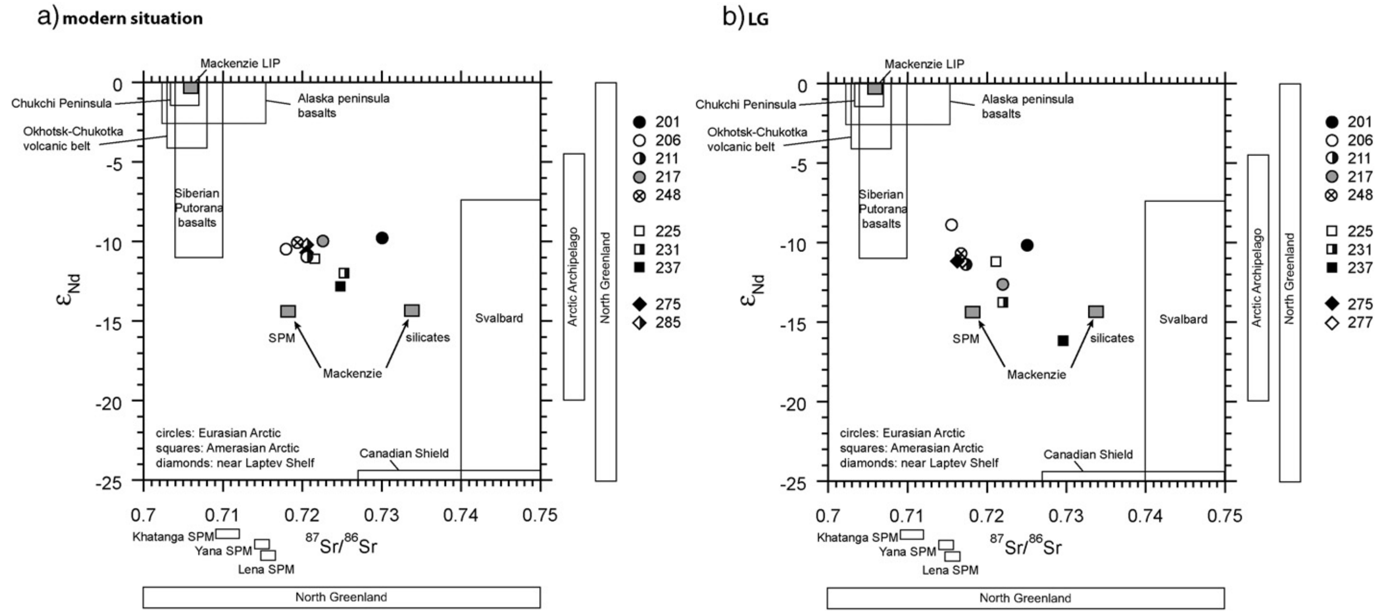

Fig. 5. ε_{Nd} versus $^{87}Sr/^{86}Sr$ diagram for the lithogenic fraction of a) surface sediments, b) sediments from the Last Glacial. Reference data for potential source areas: Siberian Putorana basalts: (Lightfoot et al., 1993; Wooden et al., 1993). Chukchi peninsula: (Ledneva et al., 2011) (from Georoc database); (Akinin et al., 2013). Okhotsk–Chukotka volcanic belt: (Tikhomirov et al., 2006). Alaska peninsula: (Andronikov and Mukasa, 2010; Akinin et al., 2013. Mackenzie particles: Goldstein et al., 1984; Millot et al., 2003). (Mackenzie LIP: Dupuy et al., 1992. Svalbard: Johansson et al., 1995; Johansson and Gee, 1999). Canadian Shield: (McCulloch and Wasserburg, 1978). North Greenland: (Kalsbeek and Jepsen, 1983, 1984; Estrada et al., 2001; Upton et al., 2005; Kalsbeek and Frei, 2006; Thorarinsson et al., 2011). Arctic Archipelago: (Patchett et al., 2004) (only ε_{Nd} values). Khatanga/Lena/Yana suspended particulate matter (SPM): (Eisenhauer et al., 1999) (only $^{87}Sr/^{86}Sr$ values).

Atlantic Deep Water formation was active during glacials. In part our results are consistent with the study by Thornalley et al. (2015). The authors found a very poorly ventilated deep Arctic Ocean during the LG based on reconstructions of deep water ventilation ages. However, an absence of deep convection, as stated by these authors, cannot be confirmed by our results. We conclude therefore that the Arctic Ocean had at least a small influence on overturning in the Nordic Seas during the LG.

4.3. Lithogenic material

4.3.1. Modern situation

The different Nd and Sr isotope compositions of the studied lithogenic fractions (Figs. 5, 6) show that the core sites are influenced by different sources. Possible transport mechanisms are erosion, river input, and sea ice transport and therefore surface

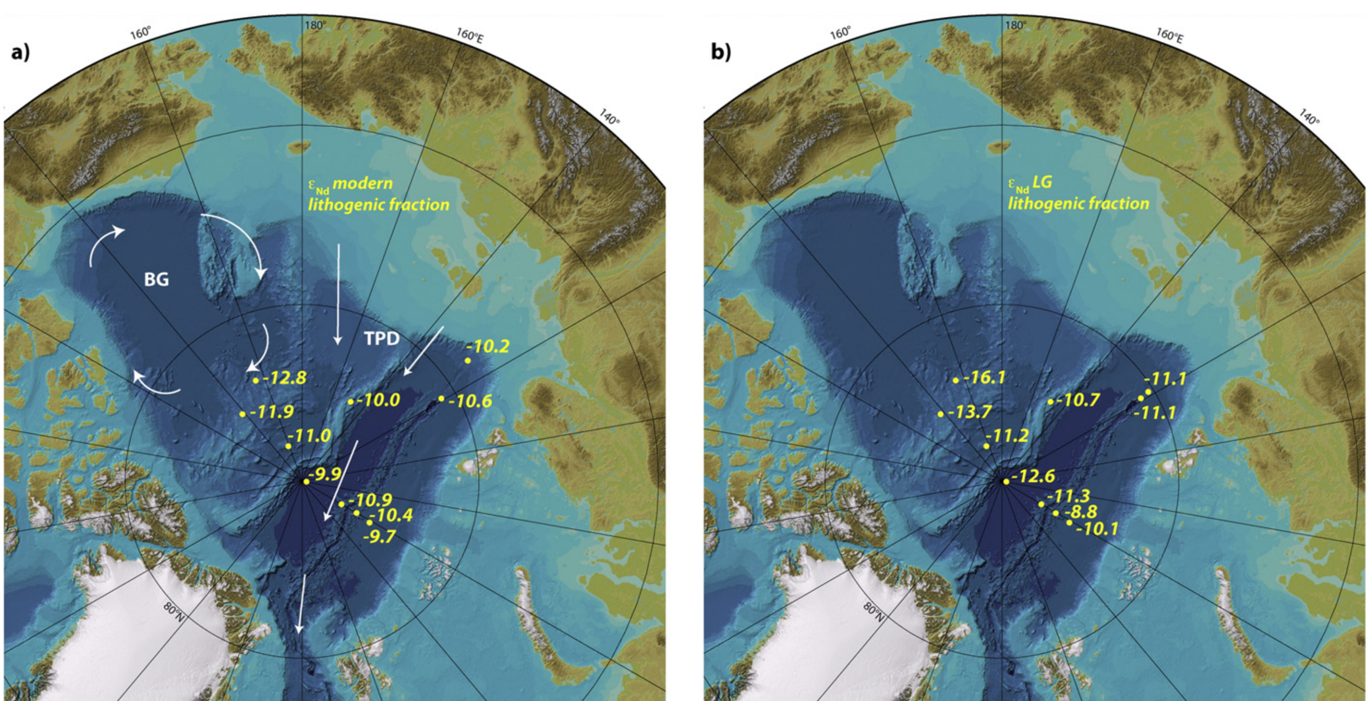

Fig. 6. (based on IBCAO, Jakobsson et al., 2008) ε_{Nd} values of the lithogenic fraction from a) surface sediments, b) sediments from the Last Glacial. Modern surface water circulations (BG Beaufort Gyre and TPD Transpolar Drift) are shown schematically.

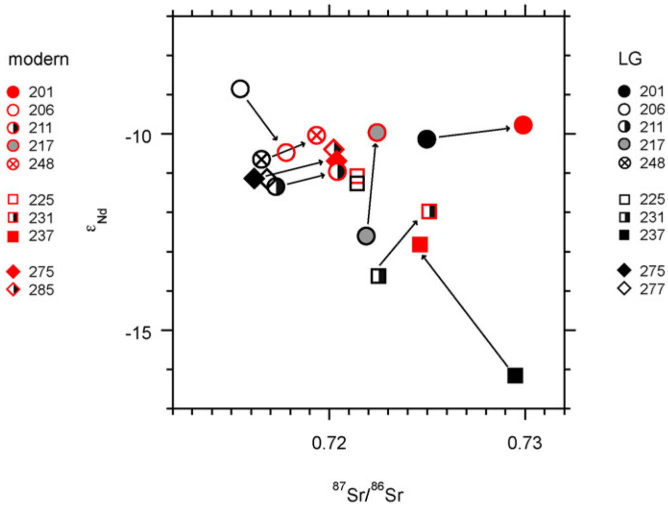

Fig. 7. Enlarged section of Fig. 5 with arrows pointing from the LG values towards the modern values for each core. Red: modern samples, black: LG samples.

currents. Eolian input plays only a minor role in the Arctic Ocean (Stein, 2008).

Individual source areas have a wide range of ε_{Nd} and $^{87}Sr/^{86}Sr$ signatures, making the assignment of our samples to distinct source areas difficult. All studied sediments most likely represent mixtures of material from the Eurasian and Amerasian Arctic.

North Greenland source rock data (ε_{Nd} and $^{87}Sr/^{86}Sr$) encompass the whole scale shown in Fig. 5 and therefore all samples could have been influenced by material from Greenland (Kalsbeek and Jepsen, 1983, 1984; Estrada et al., 2001; Upton et al., 2005; Kalsbeek and Frei, 2006; Thorarinsson et al., 2011). The same is valid for available ε_{Nd} data from the Arctic Archipelago. However, based on their location and the prevailing surface currents it is more likely that cores from the Canada Basin (231, 237) received more material from the Arctic Archipelago than cores in the Eurasian Basin (201, 206, 211, 275, 285).

Core 201 in the Nansen Basin can be distinguished from the other cores (206, 211, 248, 275, 285) of the Eurasian Basin. The high $^{87}Sr/^{86}Sr$ values are indicative of contributions from Svalbard. Svalbard source rocks have $^{87}Sr/^{86}Sr$ values ≥0.74 and ε_{Nd} from −25 to −7 (Johansson et al., 1995; Johansson and Gee, 1999). The possible transport pathway is the West Spitsbergen Current, which enters the Arctic Ocean from the Atlantic and flows along the shelf break into the Nansen Basin (Rudels et al., 2012). This current may transport sea ice with entrained material from Svalbard to station 201.

Core 225 is slightly shifted to higher $^{87}Sr/^{86}Sr$ values and lower ε_{Nd} compared to the other Eurasian cores, in accordance with its location in the Makarov Basin closer to Canada.

Cores 201, 231, and 237 are least influenced by SPM from the Siberian rivers. This can be explained by enhanced inputs from Svalbard to core 201 and the large distance of cores 231 and 237 to the Siberian coast. Cores 231 and 237 plot closer to the Mackenzie particles. The Ca/Al, Mg/Al, and TIC data provide additional evidence that locations 231 and 237 have Canadian influence especially transported by the BG (see chapter 4.1).

Our results agree with previous provenance studies that used other proxies like the chemical composition of sea ice-transported Fe oxide grains. Darby (2003) found that grains sampled from modern central Arctic ice floes have mixed sources (two Siberian sources and Banks Island in northern Canada).

4.3.2. LG

There are some clear deviations in sediment provenance from the LG to today (Figs. 5, 7). Most of the LG samples have lower $^{87}Sr/^{86}Sr$ values and lower ε_{Nd} values.

Core 201 received a smaller contribution from Svalbard. During the LG, Svalbard was covered by the Svalbard-Barents Sea Ice Sheet (Landvik et al., 1998; Svendsen et al., 2004), which, together with a lower sea level, limited sediment transport to the Arctic Ocean.

Higher ε_{Nd} values and lower $^{87}Sr/^{86}Sr$ in core 206 from the Gakkel Ridge may be explained by increased influence of basalts from this spreading ridge. Mühe et al. (1997) found ε_{Nd} values of +7 for glasses from the Gakkel Ridge. This influence could have been higher during the LG, when the external hydrological material input to the Arctic Ocean was smaller. Another possibility for higher ε_{Nd} values is an increased influence of volcanic material. Volcanic contribution from circum-Arctic sources should have ε_{Nd} values higher than −1.4 (Fagel et al., 2014 and references therein). However, the influence of basalts seems more likely because volcanic input probably would have influenced other locations as well.

Core 217 from the North Pole may have received more material from the western Arctic than today, because ε_{Nd} is shifted to lower values, which is indicative for the Mackenzie.

Cores 211, 248, 275, and 277 plot closely together and can be discriminated from the other samples by their low ε_{Nd} and $^{87}Sr/^{86}Sr$. They probably received higher contributions from Siberian basalts compared to today and compared to the other locations. The most probable transport pathway is sediment entrainment on the shelves into drifting pack ice with the TPD (Stokes et al., 2005).

The changes in ε_{Nd} and $^{87}Sr/^{86}Sr$ for core 225 from the Makarov Basin are within the measurement uncertainty. Either the transport ways of lithogenic material to this location has not changed since the LG or varying contributions from different source areas yield the same values.

Cores 231 and 237 from the Canada Basin show a greater influence from particulate material from the Mackenzie and possibly the Canadian Shield during the LG (Fig. 5). This material was most probably transported with the BG.

During the LG the Beaufort Gyre was weakened and icebergs drifted from the western Arctic ice sheets towards Fram Strait (Bischof and Darby, 1997). The transport of enclosed material with North American signatures throughout the Central Arctic Ocean was possible. At the same time, sea ice from Russia drifted towards the western Arctic north of the Arctic Archipelago before leaving the Arctic Ocean via Fram Strait as well (Bischof and Darby, 1997). The transport of material with mixed sources to the studied sediments was therefore also enabled during the LG.

5. Conclusions

The Nd and Sr isotopic composition of the leachable and lithogenic fractions of modern and LG Arctic Ocean sediments was investigated to document changes in deep water circulation and sediment provenance. The authigenic Nd isotopic signature of the surface sediments is mostly homogenous ($\varepsilon_{Nd} = -10.6 \pm 0.3$; except for one value) and implies that the modern deep water in the Eurasian Basin of the Arctic Ocean originates mainly from the North Atlantic, which is in agreement with previous studies. During the LG the authigenic fraction shows more heterogenous values. This suggests enhanced input from the shelf regions via brine rejection, while the large-scale deep water circulation does not seem to have changed, but was likely more sluggish. We suggest that the Arctic Ocean had at least a small influence on deep water formation and overturning in the Nordic Seas during the LG. Additionally, the inflow from the Makarov (Canada) Basin to the Amundsen Basin through a Lomonosov Ridge intra-basin was possibly enhanced.

Nd and Sr isotope ratios as well as bulk geochemical data indicate that the lithogenic sediment fraction represents a complex mixture from different source areas (North Greenland, Arctic Archipelago, Mackenzie area, Canadian Shield, Svalbard, as well as Eurasian sources like the Putorana basalts or the Okhotsk–Chukotka volcanic belt). The separation of the Arctic Ocean into the Amerasian and Eurasian Basins is clearly found in the isotopic signatures of the lithogenic sediment fraction. Cores located in the Amerasian Basin have higher $^{87}Sr/^{86}Sr$ values and lower ε_{Nd} indicating influence from the Mackenzie whereas cores from the Eurasian Basin have lower $^{87}Sr/^{86}Sr$ values and higher ε_{Nd} indicative of higher contributions from Siberian basalts. Additionally, higher contents of Ca, Mg, and TIC, indicative for the occurrence of dolomite from the Arctic Archipelago, and higher Mn/Al values, possible indicators for enhanced riverine input from the Mackenzie area, can be found in samples from the Amerasian Basin. Most of the lithogenic LG samples have lower ε_{Nd} and $^{87}Sr/^{86}Sr$ values than the recent samples and a less homogenous provenance signature, suggesting enhanced local input. We propose that due to lower sea level and exposed shelves, the transport pathways of lithogenic material to the Arctic Ocean were shorter, creating more heterogenous Nd and Sr isotope signatures across the Arctic basins. This diverse ε_{Nd} and $^{87}Sr/^{86}Sr$ distribution became more uniform after the LG as a result of retreating ice cover, enhanced hydrological and particle flux and deep water mixing. To further discriminate sources, studies of REE patterns of the lithogenic sediment fraction after leaching may give additional information.

Acknowledgments

The authors would like to thank the master, crew, and shipboard scientists onboard R/V *Polarstern* during the ARK-XXVI/3 expedition, M. Schulz, E. Gründken, and C. Lehners for the substantial analytical assistance, and C. März for helpful comments. Comments by C. Chauvel and two anonymous reviewers helped to improve the manuscript. This study was supported by the German Research Foundation (DFG grant, BR 775/27-1) within the IODP SPP, which is gratefully acknowledged.

References

Aagaard, K., Swift, J.H., Carmack, E.C., 1985. Thermohaline circulation in the Arctic Mediterranean Seas. J. Geophys. Res. 90 (C3), 4833–4846.

Akinin, V.V., Andronikov, A.V., Mukasa, S.B., Miller, E.L., 2013. Cretaceous lower crust of the continental margins of the northern pacific: petrological and geochronological data on lower to middle crustal xenoliths. Petrology 21 (1), 28–65.

Andronikov, A.V., Mukasa, S.B., 2010. $^{40}Ar/^{39}Ar$ eruption ages and geochemical characteristics of Late Tertiary to Quaternary intraplate and arc-related lavas in interior Alaska. Lithos 115 (1–4), 1–14.

Backman, J., Jakobsson, M., Løvlie, R., Polyak, L., Febo, L.A., 2004. Is the Central Arctic Ocean a sediment starved basin? Quat. Sci. Rev. 23 (11–13), 1435–1454.

Bayon, G., German, C.R., Boella, R.M., Milton, J.A., Taylor, R.N., Nesbitt, R.W., 2002. An improved method for extracting marine sediment fractions and its application to Sr and Nd isotopic analysis. Chem. Geol. 187 (3–4), 179–199.

Bischof, J.F., Darby, D.A., 1997. Mid- to Late Pleistocene ice drift in the western Arctic Ocean: evidence for a different circulation in the past. Science 277 (5322), 74–78.

Bischof, J., Clark, D.L., Vincent, J.S., 1996. Origin of ice-rafted debris: Pleistocene paleoceanography in the western Arctic Ocean. Paleoceanography 11 (6), 743–756.

Björk, G., Jakobsson, M., Rudes, B., Swift, J.H., Anderson, L., Darby, D.A., Backman, J., Coakley, B., Winsor, P., Polyak, L., Edwards, M., 2007. Bathymetry and deep-water exchange across the central Lomonosov Ridge at 88–89 degrees N. Deep Sea Res., Part I 54 (8), 1197–1208.

Broecker, W.S., Denton, G.H., 1989. The role of ocean–atmosphere reorganizations in glacial cycles. Geochim. Cosmochim. Acta 53 (10), 2465–2501.

Brumsack, H.-J., 2006. The trace metal content of recent organic carbon-rich sediments: implications for Cretaceous black shale formation. Palaeogeogr. Palaeoclimatol. Palaeoecol. 232 (2–4), 344–361.

Chester, R., Hughes, M.J., 1967. A chemical technique for the separation of ferro-manganese minerals, carbonate minerals and adsorbed trace elements from pelagic sediments. Chem. Geol. 2, 249–262.

Dahlqvist, R., Andersson, P.S., Porcelli, D., 2007. Nd Isotopes in Bering Strait and Chukchi Sea Waters. Goldschmidt Conf. Abstr. A196.

Darby, D.A., 2003. Sources of sediment found in sea ice from the western Arctic Ocean, new insights into processes of entrainment and drift patterns. J. Geophys. Res. Oceans 108 (C8), 3257.

Darby, D.A., Polyak, L., Bauch, H.A., 2006. Past glacial and interglacial conditions in the Arctic Ocean and marginal seas — a review. Prog. Oceanogr. 71 (2–4), 129–144.

Driscoll, N.W., Haug, G.H., 1998. A short circuit in thermohaline circulation: a cause for northern hemisphere glaciation? Science 282 (5388), 436–438.

Dupuy, C., Michard, A., Dostal, J., Dautel, D., Baragar, W.R.A., 1992. Proterozoic flood basalts from the Coppermine River area, Northwest Territories: isotope and trace element geochemistry. Can. J. Earth Sci. 29 (9), 1937–1943.

Eckert, S., Brumsack, H.-J., Severmann, S., Schnetger, B., März, C., Fröllje, H., 2013. Establishment of euxinic conditions in the Holocene Black Sea. Geology 41 (4), 431–434.

Eisenhauer, A., Meyer, H., Rachold, V., Tütken, T., Wiegand, B., Hansen, B.T., Spielhagen, R.F., Lindemann, F., Kassens, H., 1999. Grain size separation and sediment mixing in Arctic Ocean sediments: evidence from the strontium isotope systematic. Chem. Geol. 158 (3–4), 173–188.

Estrada, S., Höhndorf, A., Henjes-Kunst, F., 2001. Cretaceous/Tertiary volcanism in North Greenland: the Kap Washington Group. Polarforschung 69, 17–23.

Fagel, N., Not, C., Gueibe, J., Mattielli, N., Bazhenova, E., 2014. Late Quaternary evolution of sediment provenances in the Central Arctic Ocean: mineral assemblage, trace element composition and Nd and Pb isotope fingerprints of detrital fraction from the Northern Mendeleev Ridge. Quat. Sci. Rev. 92, 140–154.

Frank, M., 2002. Radiogenic isotopes: tracers of past ocean circulation and erosional input. Rev. Geophys. 40 (1), 1–38.

Goldstein, S.L., Onions, R.K., Hamilton, P.J., 1984. A Sm–Nd isotopic study of atmospheric dusts and particulates from major river systems. Earth Planet. Sci. Lett. 70 (2), 221–236.

Gutjahr, M., Frank, M., Stirling, C.H., Klemm, V., van de Flierdt, T., Halliday, A.N., 2007. Reliable extraction of a deepwater trace metal isotope signal from Fe–Mn oxyhydroxide coatings of marine sediments. Chem. Geol. 242 (3–4), 351–370.

Haley, B.A., Polyak, L., 2013. Pre-modern Arctic Ocean circulation from surface sediment neodymium isotopes. Geophys. Res. Lett. 40 (5), 893–897.

Haley, B.A., Frank, M., Spielhagen, R.F., Eisenhauer, A., 2008a. Influence of brine formation on Arctic Ocean circulation over the past 15 million years. Nat. Geosci. 1 (1), 68–72.

Haley, B.A., Frank, M., Spielhagen, R.F., Fietzke, J., 2008b. Radiogenic isotope record of Arctic Ocean circulation and weathering inputs of the past 15 million years. Paleoceanography 23 (1), PA1S13.

Jacobsen, S.B., Wasserburg, G.J., 1980. Sm–Nd isotopic evolution of chondrites. Earth Planet. Sci. Lett. 50 (1), 139–155.

Jakobsson, M., Andreassen, K., Bjarnadøttir, L.R., Dove, D., Dowdeswell, J.A., England, J.H., Funder, S., Hogan, K., Ingølfsson, Ó., Jennings, A., Larsen, N.K., Kirchner, N., Landvik, J.Y., Mayer, L., Mikkelsen, N., Möller, P., Niessen, F., Nilsson, J., O'Regan, M., Polyak, L., Nørgaard-Pedersen, N., Stein, R., 2014. Arctic Ocean glacial history. Quat. Sci. Rev. 92, 40–67.

Jakobsson, M., Løvlie, R., Al-Hanbali, H., Arnold, E., Backman, J., Morth, M., 2000. Manganese and color cycles in Arctic Ocean sediments constrain Pleistocene chronology. Geology 28 (1), 23–26.

Jakobsson, M., Macnab, R., Mayer, L., Anderson, R., Edwards, M., Hatzky, J., Schenke, H.W., Johnson, P., 2008. An improved bathymetric portrayal of the Arctic Ocean: implications for ocean modeling and geological, geophysical and oceanographic analyses. Geophys. Res. Lett. 35 (7), L07602.

Jang, K., Han, Y., Huh, Y., Nam, S.-I., Stein, R., Mackensen, A., Matthiessen, J., 2013. Glacial freshwater discharge events recorded by authigenic neodymium isotopes in sediments from the Mendeleev Ridge, western Arctic Ocean. Earth Planet. Sci. Lett. 369, 148–157.

Johansson, A., Gee, D.G., 1999. The late Palaeoproterozoic Eskolabreen granitoids of southern Ny Friesland, Svalbard Caledonides — geochemistry, age, and origin. GFF 121, 113–126.

Johansson, A., Gee, D.G., Björklund, L., Witt-Nilsson, P., 1995. Isotope studies of granitoids from the Bangenhuk Formation, Ny-Friesland Caledonides, Svalbard. Geol. Mag. 132 (3), 303–320.

Kalsbeek, F., Frei, R., 2006. The Mesoproterozoic Midsommersø dolerites and associated high-silica intrusions, North Greenland: crustal melting, contamination and hydrothermal alteration. Contrib. Mineral. Petrol. 152 (1), 89–110.

Kalsbeek, F., Jepsen, H.F., 1983. The Midsommersø dolerites and associated intrusions in the Proterozoic platform of Eastern North Greenland — a study of the interaction between intrusive basic magma and sialic crust. J. Petrol. 24 (4), 605–634.

Kalsbeek, F., Jepsen, H.F., 1984. The Late Proterozoic Zig-Zag Dal Basalt Formation of Eastern North Greenland. J. Petrol. 25 (3), 644–664.

Landvik, J.Y., Bondevik, S., Elverhøi, A., Fjeldskaar, W., Mangerud, J., Salvigsen, O., Siegert, M.J., Svendsen, J.-I., Vorren, T.O., 1998. The last glacial maximum of Svalbard and the Barents Sea area: ice sheet extent and configuration. Quat. Sci. Rev. 17 (1–3), 43–75.

Ledneva, G.V., Pease, V.L., Sokolov, S.D., 2011. Permo-Triassic hypabyssal mafic intrusions and associated tholeiitic basalts of the Kolyuchinskaya Bay, Chukotka (NE Russia): links to the Siberian LIP. J. Asian Earth Sci. 40 (3), 737–745.

Li, Y.H., Bischoff, J., Mathieu, G., 1969. The migration of manganese in the Arctic Basin sediment. Earth Planet. Sci. Lett. 7 (3), 265–270.

Lightfoot, P.C., Hawkesworth, C.J., Hergt, J., Naldrett, A.J., Gorbachev, N.S., Fedorenko, V.A., Doherty, W., 1993. Remobilization of the continental lithosphere by a mantle plume: major-, trace-element, and Sr-, Nd-, and Pb-isotope evidence from picritic and tholeiitic lavas of the Noril'sk District, Siberian Trap, Russia. Contrib. Mineral. Petrol. 114 (2), 171–188.

Löwemark, L., März, C., O'Regan, M., Gyllencreutz, R., 2014. Arctic Ocean Mn-stratigraphy: genesis, synthesis and inter-basin correlation. Quat. Sci. Rev. 92, 97–111.

Maccali, J., Hillaire-Marcel, C., Carignan, J., Reisberg, L.C., 2013. Geochemical signatures of sediments documenting Arctic sea-ice and water mass export through Fram Strait since the Last Glacial Maximum. Quat. Sci. Rev. 64, 136–151.

Macdonald, R.W., Gobeil, C., 2012. Manganese sources and sinks in the Arctic Ocean with reference to periodic enrichments in basin sediments. Aquat. Geochem. 18 (6), 565–591.

März, C., Stratmann, A., Matthiessen, J., Meinhardt, A.-K., Eckert, S., Schnetger, B., Vogt, C., Stein, R., Brumsack, H.-J., 2011. Manganese-rich brown layers in Arctic Ocean sediments: composition, formation mechanisms, and diagenetic overprint. Geochim. Cosmochim. Acta 75 (23), 7668–7687.

McCulloch, M.T., Wasserburg, G.J., 1978. Sm–Nd and Rb–Sr chronology of continental crust formation. Science 200 (4345), 1003–1011.

Meinhardt, A.-K., März, C., Schuth, S., Lettmann, K., Schnetger, B., Wolff, J.-O., Brumsack, H.-J., 2016. Diagenetic regimes in Arctic Ocean sediments: implications for sediment geochemistry and core correlation. Geochim. Cosmochim. Acta (in review).

Meinhardt, A.-K., März, C., Stein, R., Brumsack, H.-J., 2014. Regional variations in sediment geochemistry on a transect across the Mendeleev Ridge (Arctic Ocean). Chem. Geol. 369, 1–11.

Millot, R., Gaillardet, J., Dupre, B., Allegre, C.J., 2003. Northern latitude chemical weathering rates: clues from the Mackenzie River Basin, Canada. Geochim. Cosmochim. Acta 67 (7), 1305–1329.

Mühe, R., Bohrmann, H., Garbe-Schönberg, D., Kassens, H., 1997. E-MORB glasses from the Gakkel Ridge (Arctic Ocean) at 87°N: evidence for the Earth's most northerly volcanic activity. Earth Planet. Sci. Lett. 152 (1–4), 1–9.

Nansen, F., 1906. Northern Waters: Captain Roald Amundsen's oceanograpic observations in the Arctic Seas in 1901. Videnskab-Selskabets Skrifter 1. Mathematisk-Naturv. Klasse 3 (145 pp.).

Patchett, P.J., Embry, A.F., Ross, G.M., Beauchamp, B., Harrison, J.C., Mayr, U., Isachsen, C.E., Rosenberg, E.J., Spence, G.O., 2004. Sedimentary cover of the Canadian shield through Mesozoic time reflected by Nd isotopic and geochemical results for the Sverdrup Basin, Arctic Canada. J. Geol. 112 (1), 39–57.

Piepgras, D.J., Wasserburg, G.J., 1987. Rare earth element transport in the western North Atlantic inferred from Nd isotopic observations. Geochim. Cosmochim. Acta 51 (5), 1257–1271.

Pin, C., Zalduegui, J.F.S., 1997. Sequential separation of light rare-earth elements, thorium and uranium by miniaturized extraction chromatography: application to isotopic analyses of silicate rocks. Anal. Chim. Acta 339 (1–2), 79–89.

Porcelli, D., Andersson, P.S., Baskaran, M., Frank, M., Björk, G., Semiletov, I., 2009. The distribution of neodymium isotopes in Arctic Ocean basins. Geochim. Cosmochim. Acta 73 (9), 2645–2659.

Rachold, V., Grigoriev, M.N., Are, F.E., Solomon, S., Reimnitz, E., Kassens, H., Antonow, M., 2000. Coastal erosion vs riverine sediment discharge in the Arctic Shelf seas. Int. J. Earth Sci. 89 (3), 450–460.

Raczek, I., Jochum, K.P., Hofmann, A.W., 2003. Neodymium and strontium isotope data for USGS reference materials BCR-1, BCR-2, BHVO-1, BHVO-2, AGV-1, AGV-2F GSP-1, GSP-2 and eight MPI-DING reference glasses. Geostand. Newslett. 27 (2), 173–179.

Rudels, B., Anderson, L., Eriksson, P., Fahrbach, E., Jakobsson, M., Jones, E.P., Melling, H., Prinsenberg, S., Schauer, U., Yao, T., 2012. Observations in the Ocean. In: Lemke, P., Jacobi, H.-W. (Eds.), Arctic Climate Change: The ACSYS Decade and Beyond. Atmospheric and Oceanographic Sciences Library 43.

Rutberg, R.L., Hemming, S.R., Goldstein, S.L., 2000. Reduced North Atlantic deep water flux to the glacial Southern Ocean inferred from neodymium isotope ratios. Nature 405 (6789), 935–938.

Schauer, U., 2012. The expedition of the research vessel "Polarstern" to the Arctic in 2011 (ARK-XXVI/3 — TransArc). Rep. Polar Mar. Res. 649.

Sharma, M., Basu, A.R., Nesterenko, G.V., 1992. Temporal Sr-, Nd- and Pb-isotopic variations in the Siberian flood basalts: implications for the plume-source characteristics. Earth Planet. Sci. Lett. 113 (3), 365–381.

Spielhagen, R.F., Baumann, K.H., Erlenkeuser, H., Nowaczyk, N.R., Nørgaard-Pedersen, N., Vogt, C., Weiel, D., 2004. Arctic Ocean deep-sea record of northern Eurasian ice sheet history. Quat. Sci. Rev. 23 (11–13), 1455–1483.

Stein, R., 2008. Arctic Ocean Sediments: Processes, Proxies, and Paleoenvironment. Developments in Marine Geology 2. Elsevier (592 pp.).

Stokes, C.R., Clark, C.D., Darby, D.A., Hodgson, D.A., 2005. Late pleistocene ice export events into the Arctic Ocean from the M'Clure Strait Ice Stream, Canadian Arctic Archipelago. Global Planet. Change 49 (3–4), 139–162.

Svendsen, J.I., Alexanderson, H., Astakhov, V.I., Demidov, I., Dowdeswell, J.A., Funder, S., Gataullin, V., Henriksen, M., Hjort, C., Houmark-Nielsen, M., Hubberten, H.W., Ingølfsson, Ó., Jakobsson, M., Kjær, K.H., Larsen, E., Lokrantz, H., Lunkka, J.P., Lyså, A., Mangerud, J., Matiouchkov, A., Murray, A., Möller, P., Niessen, F., Nikolskaya, O., Polyak, L., Saarnisto, M., Siegert, C., Siegert, M.J., Spielhagen, R.F., Stein, R., 2004. Late quaternary ice sheet history of northern Eurasia. Quat. Sci. Rev. 23 (11–13), 1229–1271.

Takei, H., Yokoyama, T., Makishima, A., Nakamura, E., 2001. Formation and suppression of AlF(3) during HF digestion of rock samples in Teflon bomb for precise trace element analyses by ICP-MS and ID-TIMS. Proc. Jpn. Acad. Ser. B Phys. Biol. Sci. 77 (1), 13–17.

Tanaka, T., Togashi, S., Kamioka, H., Amakawa, H., Kagami, H., Hamamoto, T., Yuhara, M., Orihashi, Y., Yoneda, S., Shimizu, H., Kunimaru, T., Takahashi, K., Yanagi, T., Nakano, T., Fujimaki, H., Shinjo, R., Asahara, Y., Tanimizu, M., Dragusanu, C., 2000. JNdi-1: a neodymium isotopic reference in consistency with LaJolla neodymium. Chem. Geol. 168 (3–4), 279–281.

Thirlwall, M.F., 1991. Long-term reproducibility of multicollector Sr and Nd isotope ratio analysis. Chem. Geol. 94 (2), 85–104.

Thorarinsson, S.B., Holm, P.M., Duprat, H., Tegner, C., 2011. Silicic magmatism associated with Late Cretaceous rifting in the Arctic Basin-petrogenesis of the Kap Kane sequence, the Kap Washington Group volcanics, North Greenland. Lithos 125 (1–2), 65–85.

Thornalley, D.J.R., Bauch, H.A., Gebbie, G., Guo, W., Ziegler, M., Bernasconi, S.M., Barker, S., Skinner, L.C., Yu, J., 2015. A warm and poorly ventilated deep Arctic Mediterranean during the last glacial period. Science 349 (6249), 706–710.

Tikhomirov, P.L., Akinin, V.V., Ispolatov, V.O., Alexander, P., Cherepanova, I.Y., Zagoskin, V.V., 2006. The Okhotsk-Chukotka volcanic belt: age of its northern part according to new Ar–Ar and U–Pb geochronological data. Stratigr. Geol. Correl. 14 (5), 524–537.

Tütken, T., Eisenhauer, A., Wiegand, B., Hansen, B.T., 2002. Glacial–interglacial cycles in Sr and Nd isotopic composition of Arctic marine sediments triggered by the Svalbard/Barents Sea ice sheet. Mar. Geol. 182 (3–4), 351–372.

Upton, B.G.J., Ramo, O.T., Heaman, L.M., Blichert-Toft, J., Kalsbeek, F., Barry, T.L., Jepssen, H.F., 2005. The Mesoproterozoic Zig-Zag Dal basalts and associated intrusions of eastern North Greenland: mantle plume-lithosphere interaction. Contrib. Mineral. Petrol. 149 (1), 40–56.

Wedepohl, K.H., 1971. Environmental influences on the chemical composition of shales and clays. In: Ahrens, L.H., Press, F., Runcorn, S.K., Urey, H.C. (Eds.), Physics and Chemistry of the Earth vol. 8. Pergamon Press, Oxford, pp. 307–333.

Wedepohl, K.H., 1991. The composition of the upper Earth's crust and the natural cycles of selected metals. Metals in natural raw materials. Natural resources. In: Merian, E. (Ed.), Metals and their Compounds in the Natural Environment. VCH-Verlag, Weinheim, pp. 1–17.

Winter, B.L., Johnson, C.M., Clark, D.L., 1997. Strontium, neodymium, and lead isotope variations of authigenic and silicate sediment components from the Late Cenozoic Arctic Ocean: implications for sediment provenance and the source of trace metals in seawater. Geochim. Cosmochim. Acta 61 (19), 4181–4200.

Wooden, J.L., Czamanske, G.K., Fedorenko, V.A., Arndt, N.T., Chauvel, C., Bouse, R.M., King, B.S.W., Knight, R.J., Siems, D.F., 1993. Isotopic and trace-element constraints on mantle and crustal contributions to Siberian continental flood basalts, Noril'sk area, Siberia. Geochim. Cosmochim. Acta 57 (15), 3677–3704.

Zimmermann, B., Porcelli, D., Frank, M., Andersson, P.S., Baskaran, M., Lee, D.C., Halliday, A.N., 2009. Hafnium isotopes in Arctic Ocean water. Geochim. Cosmochim. Acta 73 (11), 3218–3233.